Atmospheric
Chemistry
and Physics
Discussions

Open Access

Climatology of the aerosol optical depth by components from the Multiangle Imaging SpectroRadiometer (MISR) and a high-resolution chemistry transport model

H. Lee[1], O. V. Kalashnikova[1], K. Suzuki[2], A. Braverman[1], M. J. Garay[1], and R. A. Kahn[3]

[1]Jet Propulsion Laboratory, California Institute of Technology, Pasadena, California, USA
[2]Atmosphere and Ocean Research Institute, University of Tokyo, Tokyo, Japan
[3]Laboratory for Atmospheres, NASA Goddard Space Flight Center, Greenbelt, Maryland, USA

Correspondence to: H. Lee (huikyo.lee@jpl.nasa.gov)

Discussion Paper | Discussion Paper | Discussion Paper | Discussion Paper |

ACPD

15, 33897–33929, 2015

AOD by component from MISR and chemistry models

H. Lee et al.

Title Page

Abstract   Introduction
Conclusions   References
Tables   Figures

|◀   ▶|
◀   ▶
Back   Close

Full Screen / Esc

Printer-friendly Version

Interactive Discussion

Full Screen / Esc

Printer-friendly Version

Interactive Discussion

Abstract

The Multi-angle Imaging SpectroRadiometer (MISR) Joint Aerosol (JOINT_AS) Level 3 product provides a global, descriptive summary of MISR Level 2 aerosol optical depth (AOD) and aerosol type information for each month between March 2000 and the present. Using Version 1 of JOINT_AS, which is based on the operational (Version 22) MISR Level 2 aerosol product, this study analyzes, for the first time, characteristics of observed and simulated distributions of AOD for three broad classes of aerosols: non-absorbing, absorbing, and non-spherical – near or downwind of their major source regions. The statistical moments (means, standard deviations, and skewnesses) and distributions of AOD by components derived from the JOINT_AS are compared with results from the SPectral RadIatioN-TrAnSport (SPRINTARS) model, a chemistry transport model (CTM) with very high spatial and temporal resolution. Overall, the AOD distributions of combined MISR aerosol types show good agreement with those from SPRINTARS. Marginal distributions of AOD for each aerosol type in both MISR and SPRINTARS show considerable high positive skewness, which indicates the importance of including extreme AOD events when comparing satellite retrievals with models. The MISR JOINT_AS product will greatly facilitate comparisons between satellite observations and model simulations of aerosols by type.

1 Introduction

Atmospheric aerosol distributions and temporal variations play fundamental roles in the Earth's climate system. Direct radiative forcing of aerosols due to scattering and absorption of shortwave radiation is estimated at around $-0.7\,\mathrm{W\,m^{-2}}$ from reanalysis data (Bellouin et al., 2013) and $-1.3\,\mathrm{W\,m^{-2}}$ based on satellite observations (Bellouin et al., 2008). In addition, aerosols affect radiative forcing indirectly by changing the microphysical properties of clouds and precipitation. Studies on the impacts of aerosols on large-scale circulation have brought further attention to interactions between aerosols

and clouds. For example, Li et al. (2008) showed that the recent positive trend in wintertime precipitation over the North Pacific is related to increased aerosol emissions. Zhang et al. (2007) and Wang et al. (2014) suggested that increased anthropogenic aerosol emissions in Asia can strengthen cyclones along the Pacific storm track. Both direct and indirect radiative forcing of aerosols are expected to be more important under a changing climate. For example, Ganor et al. (2010) and Lu et al. (2010) reported increasing dust aerosols in Africa and sulfate aerosols in China, respectively. However, global climate models (GCMs) have a hard time producing consistent radiative forcing responses to varying concentrations of aerosols (IPCC, 2013). In fact, indirect radiative forcing due to aerosols is one of the dominant sources of uncertainty in the energy budget of many GCMs (Regayre et al., 2014).

Despite substantial improvements in the representation of physical and chemical processes related to aerosols in global-scale chemistry models relative to most GCMs, recent work has shown that chemistry models still exhibit considerable biases and uncertainties in aerosol concentrations and related radiative forcings (Lee et al., 2013; Shindell et al., 2013). Therefore, validating simulated aerosols in chemistry models is critical in order to better understand the root causes of these biases and uncertainties.

Aerosol–radiation interactions are determined by the size distribution of aerosols, as well as their shape and light-absorption properties (Boucher et al., 2013). Understanding the optical and microphysical characteristics of natural and anthropogenic aerosols is critical for advancing the ability of CCMs to correctly simulate the climate impact of aerosols. Nevertheless, many previous studies evaluating simulated aerosol optical depth (AOD) in models against satellite observations, such as those available from the Moderate Resolution Imaging Spectroradiometer (MODIS) and the Multi-angle Imaging SpectroRadiometer (MISR), have used only the total column AOD without taking into account aerosol type information (e.g., Tilmes et al., 2015). Shindell et al. (2013) compared AODs for each aerosol type simulated in nine chemistry climate models (CCMs). Not surprisingly, the difference in component AODs among models is much greater than the difference in total AODs (see Fig. 3 in Shindell et al., 2013). To un-

derstand the diverse partitioning of AOD among dust, sea salt, sulfate, nitrate, black carbon, and organic carbon in CCMs, it is important to compare the simulated component AODs against global climatological maps of observed AOD by components, if possible.

Unfortunately, the retrieval of AOD by type from satellite observations and using the retrieved AOD for chemistry model evaluation have been, and remain, a significant challenge. Aerosol polarization measurement by the POLDER3 (POLarization and Directionality of the Earth Reflectance) instrument onboard the PARASOL (Polarization and Anisotropy of Reflectances for Atmospheric Sciences coupled with Observations from a Lidar) enables classifying observed aerosols into various types (Russell et al., 2014). CALIPSO (Cloud-Aerosol Lidar and Infrared Pathfinder Satellite Observation) also provides aerosol classification according to surface type (Omar et al., 2009). Higurashi and Nakajima (2002) suggested detecting a dominant aerosol type using radiances from four channels on the Sea-viewing Wide Field-of-view Sensor (SeaWiFS). Kim et al. (2007) used both MODIS observations and data from the Ozone Monitoring Instrument (OMI) to classify retrieved aerosol types, but the algorithm was similarly limited to providing a single, dominant aerosol type. In the AOD climatology by type reconstructed in Nabat et al. (2013), total AOD is from a satellite instrument, but the AOD by type was derived solely from the fractions of the five aerosol types (sulfate, black carbon, organic carbon, dust, and sea salt) simulated in two CCMs. Holzer-Popp et al. (2008) provided an overview of currently available aerosol type datasets from satellites, and used the the Advanced Along Track Scanning Radiometer (AATSR) and the Scanning Imaging Absorption Spectrometer for Atmospheric Cartography (SCIAMACHY) onboard the European Environmental Satellite (ENVISAT) to produce total column AOD and speciation by aerosol mixtures. In their study, total column AOD and surface reflectivity were derived from AATSR observations and these variables were used to simulate spectra for pre-defined aerosol mixtures, which were selected by comparison with the observed SCIAMACHY spectra.

Full Screen / Esc

Printer-friendly Version

Interactive Discussion

Due to its unique multiangle viewing approach, the MISR instrument on NASA's Terra satellite is capable of distinguishing mixtures of aerosol types without relying on data from other instruments (Diner et al., 2005a). MISR measures radiation in four spectral bands (blue – 446 nm, green – 558 nm, red – 672 nm, and near infrared – 866 nm) from nine different viewing directions (±70.5, ±60.0, ±45.6, ±26.1, and 0.0° along the direction of satellite motion), allowing retrievals of aerosol particle size and shape (Kahn et al., 2001; Diner et al., 2005b). The operational (Version 22) aerosol retrieval algorithm is based on matching observed top of atmosphere (TOA) radiances to radiances modeled for AODs ranging from 0.0 to 3.0 from 74 "mixtures" based on eight "pure" particle types, each one representing a single size distribution with specific optical properties (Kahn et al., 2010). Within the algorithm, a mixture is acceptable, or "passing," if the difference between the observed and modeled radiances are less than a pre-determined value. In the Level 2 (swath) product, the mean of the passing mixtures is reported in the field "RegBestEstimateSpectralOptDepth" at a spatial resolution of 17.6 km × 17.6 km. The best-fitting mixture out of the 74 candidates is reported as the "RegLowestResidMixture," but the AOD and information about which mixtures were considered "passing" are retained in the fields "OptDepthPerMixture" and "AerRetrSuccFlagPerMixture," respectively, for further evaluation. Validation of the Level 2 Version 22 product against ground-based observations from the Aerosol Robotic Network (AERONET) (Holben et al., 1998), including assessments of particle type retrievals, can be found in Kahn et al. (2010) and Kahn and Gaitley (2015). The mixture type information in the MISR Version 22 aerosol product has been exploited by Li et al. (2013, 2015), for example, who used CCM information to select from the complete set of "passing" mixtures to improve agreement with AERONET in the continental United States.

The main objective of the current study is to compare multi-year MISR AOD by component climatologies with simulated AODs, broken down by aerosol type. The results of this work highlight the added value of using AOD by components from MISR in evaluating chemistry transport models (CTMs) and CCMs. Due to the relatively short

lifetime of aerosols compared to trace gases, it is also important to consider the spatial inhomogeneity of aerosol distributions and resulting regional effects. Here we focus, in particular, on characterizing AOD distributions in the regions near major aerosol emission sources: East Asia, the Sahara Desert, and West Africa with comparisons between MISR climatological observations and high-resolution simulations from the the SPectral RadIatioN-TrAnSport (SPRINTARS) model for Aerosol Species (Takemura et al., 2002, 2005) interactively coupled to the Nonhydrostatic Icosahedral Atmospheric Model (NICAM) (Satoh et al., 2008, 2014; Suzuki et al., 2008). We also demonstrate why it is important to consider spatio-temporal distributions of AOD when comparing satellite observations and models rather than simply using spatially and temporally averaged AODs for model evaluation.

The remainder of the paper is structured as follows. The data and model used in this study are described in Sect. 2. Comparisons between MISR retrievals and model simulations are presented in Sect. 3, followed by a summary of key findings in Sect. 4.

2   Data

2.1   MISR Level 3 Joint Aerosol product

As more observations become available for model intercomparison projects, such as AeroCom (Schulz et al., 2006; Myhre et al., 2013), the Coupled Model Intercomparison Project Phase 5 (CMIP5) (Taylor et al., 2012), and the Atmospheric Chemistry and Climate Model Intercomparison Project (ACCMIP) (Lamarque et al., 2013), it is important that these data become more accessible (Teixeira et al., 2014). Getting the mixture information from the MISR Level 2 aerosol product is an indirect procedure, requiring access to Hierarchical Data Format (HDF) Vertex Data (VDATA) fields that map integer-valued mixture identifiers in the Level 2 files to the MISR "pure" particle types and corresponding mixing proportions. Each "pure" particle is assumed to have uniform composition and a specified size distribution. To make this information more

readily available, and to reduce the overall data volume required for large-scale analysis, the MISR project provides a Level 3 (gridded) Joint Aerosol Product (JOINT_AS) that summarizes the Level 2 aerosol retrievals on a monthly, 5° × 5° latitude–longitude spatial–temporal grid. The contents of the JOINT_AS product can be thought of as

5 eight-dimensional histograms summarizing a large number of retrievals in every grid cell. The summarization algorithm is based on Braverman and Di Girolamo (2002). Each grid cell in the product contains a set of representative vectors and their associated weights in what is essentially a multi-dimensional probability distribution. The representative vectors have eight components, which are the mid-visible (558 nm) AODs

10 corresponding to MISR's eight "pure" particle types. These eight particles are made up of four non-absorbing spherical size distributions with effective radii of 0.06, 0.12, 0.26, and 2.80 μm; two spherical absorbing size distributions both with an effective radius of 0.12 μm and single scattering albedos of 0.9 and 0.8 in the mid-visible; and two non-spherical size distributions corresponding to dust grains with an effective radius of

15 0.75 μm, and spheroids with an effective radius of 3.32 μm (Kahn et al., 2010; Kahn and Gaitley, 2015).

Conceptually, one can think of the JOINT_AS product as being created as follows. First, all "passing" mixtures in a given grid cell are transformed into an eight-vector that aggregates mixing proportions across mixtures to yield total proportions of each pure

20 particle type. Next, these proportions are multiplied by the total retrieved ("RegBestEstimateSpectralOptDepth") mid-visible AOD to create an eight-vector of AODs that sums to the total reported AOD. To summarize the multi-dimensional distribution of AOD, the JOINT_AS product uses a clustering algorithm to partition the eight vectors into groups with similar members. Detailed description on the clustering algorithm used to gener-

25 ate JOINT_AS can be found Braverman (2002). In this study, we use Version 1 of MISR JOINT_AS, based on the operational (Version 22) Level 2 MISR aerosol retrievals, for all months for the 15 years from March 2000 through February 2015.

Figure 1 shows an example of how to visualize a two-dimensional subset of the eight-dimensional histogram contained within the MISR JOINT_AS product as a scatterplot

of absorbing AOD plotted against non-absorbing AOD over East Asia for the month of April. One-dimensional sampling distributions are shown as the histogram on the top of the figure for non-absorbing particles and to the right of the figure for absorbing particles. The scatterplot itself shows how these two particle types covary with one another in this region for this time period. From the histograms, the MISR V22 product identifies non-absorbing particles as the dominant aerosol component, which tend to span the range from about 0.025 to 0.15, whereas absorbing aerosols are retrieved only for AOD values less than about 0.02, where aerosol-type retrieval sensitivity is very low (Kahn et al., 2010; Kahn and Gaitley, 2015). Because of this, there is very little covariance between the absorbing and non-absorbing AOD in this case.

From the information used to construct the marginal histograms it is simple to calculate the moments (mean, variance, and skewness) of the AOD distributions for different aerosol types. The kth central moment of the distribution (M_k) with a sample size, N, is conventionally defined as follows:

$$\text{first moment (mean)} = \overline{x} = \frac{1}{N} \sum_{j=1}^{N} x_j \tag{1}$$

$$k\text{th central moment} = M_k = \frac{1}{N} \sum_{j=1}^{N} (x_j - \overline{x})^k \tag{2}$$

where x_j corresponds to the jth AOD. Using the above definitions, the skewness of the distribution can be represented as:

$$\text{skew} = N \frac{M_3}{M_2^{1.5}}. \tag{3}$$

If the data follow a normal (Gaussian) distribution, the skewness of the data should be close to zero. If a distribution has positive skewness, the tail representing values larger than the median of the distribution is longer than the tail representing smaller values.

AOD by component from MISR and chemistry models

H. Lee et al.

Title Page

Abstract	Introduction
Conclusions	References
Tables	Figures

| ◄◄ | ►► |
| ◄ | ► |

| Back | Close |

Full Screen / Esc

Printer-friendly Version

Interactive Discussion

Conversely, if the distribution has a negative skewness, the tail representing smaller values is larger. If the skewness of the distribution is not close to zero, the mean and standard deviation are not enough to appropriately represent the distribution. However, for a normal distribution the standard deviation of the sample skewness is approximately $\sqrt{15/N}$, where N is the sample size. Skewness values less than a few times as large as this (e.g., |skew| < 3 for a sample size of 15) should be viewed with suspicion. On the other hand, when the distribution of data is highly skewed, this indicates that it is necessary to analyze individual values or at least a summary histogram of the data in order to understand how the data are actually distributed. As we will show, the ability to easily determine the moments and distributions of the MISR AODs by component is an important feature of the JOINT_AS product.

2.2 The SPRINTARS model

The SPRINTARS model coupled to high-resolution NICAM model reports AOD every three hours for four different types of aerosols (carbonaceous, dust, sea salt, and sulfate) with a horizontal resolution of 7 km globally. As described by Suzuki et al. (2008), the SPRINTARS CTM reasonably reproduced global distributions of total AOD in comparison with MODIS near major aerosol emission sources. SPRINTARS is also one of the models included the AeroCom intercomparison (Huneeus et al., 2011). Although due to computational limitations the SPRINTARS simulation period used in this study covers only eight days from 1 July through 8 July 2006, the high spatial and temporal resolution of the model output allow us to compare simulated AOD distributions with those from MISR under the assumption that the AOD distribution does not change significantly from one year to the next during the month of July ("the stationarity assumption"). We adopt this approach because we found that the JOINT_AS product for the single month of July 2006 contained a significant number of missing values even at $5° \times 5°$ spatial resolution. The missing data are likely due to cloud screening and locations being flagged as inappropriate for aerosol retrievals, as discussed in Kahn

et al. (2009). Comparison of long-term CTM simulations driven by reanalysis datasets with MISR component AODs may provide insight into the interannual variability of AOD type distributions. Specifically, the variability among the Julys from MISR might indicate how representative one July from SPRINTARS might be. However, this investigation is beyond the scope of the current work.

It is important to note that the aerosol types in SPRINTARS are different from the "pure" particle distributions used in the operational MISR aerosol retrievals. In order to make the MISR AOD by components comparable with those of the model, MISR aerosol types were combined in the manner shown in Table 1. AODs from weakly and strongly absorbing aerosols in the MISR dataset, with single scattering albedo (SSA) in the mid-visible of 0.9 and 0.8, respectively, were combined to construct an analog to modeled carbonaceous aerosols. The combination of the more absorbing and less absorbing aerosol particles is intended to represent the range of such particles in nature (e.g., Liu et al., 2014). Given the limitation of MISR to represent the modeled dust, the AODs from the non-spherical grains and coarse spheroids from MISR (Kalashnikova et al., 2005) were combined. Finally, AODs from the three (small) non-absorbing particles were added to compare to the modeled sulfate and nitrate aerosols. The largest MISR particle type, with an effective radius of 2.8 µm, was excluded when calculating the non-absorbing AOD due to issues with retrieval sensitivity to this component (Kahn et al., 2010).

3 Results

3.1 East Asia

Rapid increases in emissions of aerosols and their precursors in East Asia have caused growing concern because of the broad impact of Asian aerosols on the North Pacific and mainland North America, especially the United States (Yu et al., 2008). Figure 2 compares climatological AODs from non-absorbing aerosols for July retrieved

by MISR in East Asia with the sulfate AOD predicted by SPRINTARS for the beginning of July 2006. Panels a and b of Fig. 2 are the respective MISR non-absorbing and SPRINTARS sulfate AOD maps displayed using the same color scale. Peak AOD values correspond to source regions in the Shandong Province south of Beijing and are closely related to the emissions in this heavily industrial region (Streets et al., 2007). The spatial gradient in AOD is due to transport and deposition processes. In spite of the differences in time period, these figures show very good qualitative agreement in their representation of the spatial distribution of non-absorbing/sulfate AOD. It is worth noting that both MISR and SPRINTARS capture a secondary peak in AOD in southwestern China in Sichuan Province, which burns coal high in sulfur (Streets and Waldhoff, 2000), with peak loading seen in April, July, and October (Wang et al., 2010). The reason for this good agreement is likely that the industrial source regions are well considered in the emission database used for SPRINTARS.

Figure 2c and d shows the probability mass function (PMF) of the non-absorbing AOD from MISR and the sulfate AOD from SPRINTARS, respectively, corresponding to the shaded boxes on the maps in Fig. 2a and b. The PMF is simply the histogram scaled so that the total area of the bars corresponds to some fixed value. The boxes capture the region of highest AOD loading. It is important to recognize that Fig. 2c from MISR includes both temporal and spatial variability because it is averaged over a 15 year time period, whereas Fig. 2d from SPRINTARS represents primarily spatial variability. Even so, the histograms have similar shapes, with only a 13 % disagreement in the mean non-absorbing/sulfate AOD (0.45 for MISR and 0.39 for SPRINTARS) and similar standard deviations (0.39 for MISR and 0.35 for SPRINTARS). What is noticeable about the shapes of the distributions is that they are non-Gaussian, with long positive tails. The ability to visualize the full AOD distribution is an important analysis technique enabled by the MISR JOINT_AS product. The skewness of the MISR distribution is 1.56 and for SPRINTARS the skewness is 2.47, showing that the model has more positive skewness corresponding to more high AOD values. This is consistent with Fig. 2b, which

shows values in the box tend to be purple (AOD > 0.5) for SPRINTARS with somewhat lower values for the boxed region in the MISR climatology in Fig. 2a.

Levy et al. (2009) describe how the monthly mean AOD reported by satellite instruments is highly dependent on the averaging method selected. Reliance on the mean and standard deviation alone are particularly problematic when high outliers are common. A satellite instrument can miss extreme events due to its sampling characteristics (Colarco et al., 2014), but these events may be captured by a model with better temporal and complete spatial sampling. If this is the case, the mean AOD values could be very different, but, as shown here, the distributions are still similar.

It is worth noting that taking the base-10 logarithm of the non-absorbing/sulfate AODs in Fig. 2c and d results in distributions with skewnesses of -0.25 (MISR) and -0.26 (SPRINTARS). These skewness values are very close to zero, indicating that these modified distributions are very nearly log-normal, as is typical for atmospheric pollutant concentrations (Ott, 1990). The results in Fig. 2 as a whole indicate that combining MISR non-absorbing AOD in the manner described appears to be a good proxy for sulfate aerosol loading, at least in East Asia.

When comparing satellite-derived total column AOD with modeled AOD, it is common practice to assume that a single, dominant type of aerosol accounts for the majority of the modeled AOD in a region (e.g., Kim et al., 2007). However, this approach will not work if the dominant pollutant type varies over time (Wang et al., 2010). Another useful characteristic of the MISR operational aerosol retrieval is that the mixture climatology is applied globally to all locations and seasons, unlike MODIS over land, which relies on aerosol models that change as a function of location and season based on the AERONET climatology (Levy et al., 2013). A recent study by Eck et al. (2013), for example, showed that the seasonality in biomass-burning SSA in southern Africa is better captured by MISR than MODIS due to these different approaches. Figure 3 shows the monthly partitioning of aerosol type from MISR for April (top row) and July (bottom row) based on the 15 year climatology from the JOINT_AS product. This is possible because

the product retains statistical information on the full range of "passing" particle types within a 5˚ × 5˚ grid cell instead of reporting a single, dominant particle type.

What is immediately apparent when comparing the April and July particle type climatologies from MISR is that the dominant source region in April is located in the vicinity of Hong Kong, whereas in July it is farther to the north as discussed in relation to Fig. 2. In April the southern source region is dominated by non-absorbing aerosols (sulfate and possibly nitrate), with absorbing aerosols being a secondary contributor. Both the partitioning and seasonality are consistent with monthly observations of $PM_{2.5}$ constituents in Hong Kong (Haung et al., 2014). Additionally, there is significantly more non-spherical aerosol in the region in April, when dust storms are most frequent (e.g., Wang et al., 2010; Lee et al., 2013). Although individual dust events do not last very long, they are captured in the long-term MISR climatology due to their seasonal recurrence. Although the dust makes an important contribution to the total AOD, it would be a mistake to use the total monthly mean AOD in the region to study the transport and radiative effects of dust by itself in China. Figure 3 demonstrates the value of aerosol data from the MISR JOINT_AS product to further study climate impacts and air quality issues due to aerosols originating in East Asia.

3.2 Eastern Atlantic

The eastern Atlantic Ocean in July is directly downwind from the largest source of dust aerosols on Earth (e.g., Koven and Fung, 2008; Ridley et al., 2012). Figure 4a shows a map of the climatology of non-spherical aerosol optical depth for July from 15 years of MISR data from the JOINT_AS product for the eastern Atlantic off western Africa. Figure 4b shows the SPRINTARS-simulated dust aerosol AOD from 1 July through 8 July 2006 for the same region. We focus on retrievals over ocean because of the highly episodic nature of dust events (e.g., Ben-Ami et al., 2012) (see also Fig. 5), which make direct comparisons difficult in the source regions themselves. In addition, although MISR-reported AODs show good agreement with AERONET in this region, the magnitude tends to be underestimated in situations with high aerosol loading, as in

the case of large dust outbreaks (Kahn et al., 2010; Carboni et al., 2012; Banks et al., 2013). On the modeling side, in the first AEROCOM intercomparison, the SPRINTARS model also tends to underestimate the emissions in north Africa, with dust particles having too short a lifetime (1.6 days) (Huneeus et al., 2011). In this regard, it is impor-
5 tant to recall that the MISR data represent a temporal average over 15 years, whereas the SPRINTARS model is likely representing a single, large dust event. In spite of these differences, there is generally good agreement between the maps in Fig. 4a and b. The latitudinal spread is less in the model than in the climatology, whereas the longitudinal extent of high dust AOD loading is greater in the MISR climatology. Between the
10 end of March and mid-October, the location of the maximum dust emission shifted with time, consistent with the differences shown here in the latitudinal distributions (Prospero et al., 2002; Ben-Ami et al., 2012). The difference in longitudinal extent could be related to the lifetime of the dust particles in the SPRINTARS model (Huneeus et al., 2011).
15   Focusing on the shaded rectangles on the two maps, Fig. 4c and d shows the PMFs of the non-spherical AOD from MISR and dust AOD from SPRINTARS. The two distributions have similar means (0.37 for MISR and 0.35 for SPRINTARS) and standard deviations (0.21 for MISR and 0.18 for SPRINTARS). Both distributions also have significant positive skewness (0.97 for MISR and 1.56 for SPRINTARS), with the model
20 showing much greater skewness than the satellite observations. Looking at the distributions themselves, it is apparent that the model distribution, which is dominated by spatial variability, is much better behaved than the MISR distribution, which contains contributions from both spatial and temporal variability. Although the peaks of the two distributions are nearly identical (0.350 for MISR and 0.325 for SPRINTARS),
25 the SPRINTARS distribution is much more sharply peaked. The MISR distribution appears to have a secondary peak around 0.2, that is not represented in the SPRINTARS distribution, which instead has a peak around 0.075. Careful inspection of the two distributions shows that frequency of AOD values larger than the highest peak in the SPRINTARS model falls off more rapidly than they do in the MISR observations, an-

Title Page

Abstract | Introduction

Conclusions | References

Tables | Figures

|◀ | ▶|

◀ | ▶

Back | Close

Full Screen / Esc

Printer-friendly Version

Interactive Discussion

other indication that the dust lifetime may be too short in the model. Again, this demonstrates the importance of comparing probability distributions in AOD between models and observations rather than relying on differences in mean AODs as a performance metric.

Figure 5 shows the non-spherical AOD climatology for north Africa for July for 2000 to 2014 from the MISR JOINT_AS product at 5° resolution. What is immediately apparent is the significant interannual variability in both dust loading and peak locations. The western Sahara is particularly variable in both location and intensity, but the region downwind from the Bodélé Depression in Chad (Bristow et al., 2009), around 10° E, is persistent, but with varying intensity from year to year. This indicates that in north Africa, the stationarity assumption for the spatial distribution of non-spherical AOD does not work well. Therefore, if simulation datasets are available for a longer period, it is important to compare the temporal and spatial variability of the modeled dust AOD with MISR for each year.

3.3 Western Africa

Over half of the global emissions of carbon come from Africa (van der Werf et al., 2010) and in western Africa, south of the Equator, these emissions are dominated by savanna and grassland fires (Ichoku and Ellison, 2014). Figure 6a shows the MISR absorbing aerosol climatology for July from 15 years of data from the JOINT_AS product. Figure 6b is the same region showing the carbonaceous aerosols from the SPRINT-ARS model from 1 July through 8 July 2006. At first glance, the agreement between the satellite observations and the model appears to be quite good. However, more careful examination shows that the highest aerosol loading predicted by the SPRINT-ARS model occurs primarily over northwestern Angola and the Democratic Republic of the Congo compared to the satellite data, which has a maximum extending from the Atlantic Ocean, across the Republic of the Congo, into the Democratic Republic of the Congo. The modeled carbonaceous aerosols are therefore displaced to the southeast relative to the MISR satellite observations. A similar displacement was

H. Lee et al.

Title Page

Abstract | Introduction

Conclusions | References

Tables | Figures

|◄ | ►|

◄ | ►

Back | Close

Full Screen / Esc

Printer-friendly Version

Interactive Discussion

found by Liousse et al. (2010) when comparing POLarization and Directionality of the Earth's Radiation (POLDER) total column AOD measurements from the Polarization and Anisotropy of Reflectances for Atmospheric Sciences coupled with Observations from a Lidar (PARASOL) satellite with modeled AOD for July 2006. These authors at-

5 tribute the displacement to errors in the location of the biomass burning emissions, errors in transport, or errors in the satellite products. In fact, the location of the maximum SPRINTARS carbonaceous AOD corresponds well with the location of the maximum BC emission in the Global Emissions Inventory Activities (GEIA) emissions (Liousse et al., 2010), which are used in the SPRINTARS model (Takemura et al., 2005). The

10 GEIA emissions distribution in this region is consistent with version 3 of the Global Fire Emissions Database (GFED3) (van der Werf et al., 2010) as well as the Fire Energetics and Emissions Research version 1.0 (FEER.v1) (Ichoku and Ellison, 2014) database. The spatial distribution of absorbing aerosols from MISR shown in Fig. 6a is also consistent with the AOD map from POLDER shown in Liousse et al. (2010), even

15 though the PARASOL satellite has a 13:30 LT equatorial crossing time compared to the 10:30 LT equatorial crossing time for the Terra satellite. These results implicate the transport and deposition processes in the SPRINTARS model, as opposed to the emissions inventory or the satellite products, themselves. Even so, recent work by Marlier et al. (2014) has shown that daily fire emissions lead to different model results com-

20 pared to monthly fire emissions, and Veira et al. (2015) show that the injection height of aerosols can also play a role in the modeled distribution of AOD from biomass burning. The paper by Matichuk et al. (2007) includes a longer list of additional model sensitivities that complicate model predictions of carbonaceous aerosol loading, particularly in transport regions.

25 Figure 6c and d shows the distribution of absorbing/carbonaceous AOD from MISR and SPRINTARS for the shaded box on the maps in Fig. 6a and b, which corresponds to the region of highest AOD loading in both the observations and the model. In this case, the two distributions are quite similar. The mean MISR AOD is 0.37, and the mean SPRINTARS AOD is 0.33, with the difference likely due to the broader spatial distribu-

tion of the absorbing aerosols in the MISR observations over 15 years compared to the eight days of the SPRINTARS model run. The peak values in the two distributions are also similar, around 0.2, with the SPRINTARS peak shifted slightly higher. The standard deviations for MISR and SPRINTARS are 0.22 and 0.20, respectively, with the MISR distribution skewed slightly higher with a skewness of 0.72, compared to 0.63 for SPRINTARS. These results are consistent with the SPRINTARS model producing carbonaceous aerosols that are not transported sufficiently far given their lifetime in the model. Again, the ability to generate distributions of AOD by aerosol type is an important strength of the MISR JOINT_AS product and, as shown in this example, provides a powerful model diagnostic.

4   Conclusions

Although a number of previous studies have evaluated aerosols modeled in both GCMs and chemistry models using observational datasets from a variety of sources, studies focusing on specific aerosol types have been limited by the lack of global comparison datasets. However, it is well understood that model improvements depend on moving beyond simple comparisons of total AOD. In this work, we describe the MISR Level 3 Joint Aerosol product that provides monthly climatological distributions of AOD for eight different aerosol types, which allows detailed statistical comparisons between satellite observations and models. In addition we demonstrated how the MISR "pure" particle types can be combined into analogs for model aerosol species. In comparisons with the SPRINTARS model we showed that reliance on the simple mean and standard deviation of the AOD distribution can lead to misleading conclusions. In every case, high positive skewness in the distributions is indicative of large outliers that may be due to episodic events or differences in sampling that must be considered when making comparisons between satellite observations and model datasets. We also showed how the reliance on a single, dominant aerosol type may be inappropriate for certain locations and seasons.

We believe that the comparison of AOD distributions by components between MISR and chemistry models will provide useful guidance to improve model emissions, transport processes, and ultimately improve computations of aerosol-related radiative forcing in the models. Further research along these lines would clarify uncertainties of chemistry models on regional and global scales. Conversely, scrutinizing the AOD distributions reported by MISR using chemistry climate models may feed back and improve the quality of aerosol retrievals from MISR.

References

Banks, J. R., Brindley, H. E., Flamant, C., Garay, M. J., Hsu, N. C., Kalashnikova, O. V., Klüser, L., and Sayer, A. M.: Intercomparison of satellite dust retrieval products over the west African Sahara during the Fennec campaign in June 2011, Remote Sens. Environ., 136, 99–116, doi:10.1016/j.rse.2013.05.003, 2013. 33910

Bellouin, N., Jones, A., Haywood, J., and Christopher, S. A.: Updated estimate of aerosol direct radiative forcing from satellite observations and comparison against the Hadley Centre climate model, J. Geophys. Res., 113, D10205, doi:10.1029/2007jd009385, 2008. 33898

Bellouin, N., Quaas, J., Morcrette, J.-J., and Boucher, O.: Estimates of aerosol radiative forcing from the MACC re-analysis, Atmos. Chem. Phys., 13, 2045–2062, doi:10.5194/acp-13-2045-2013, 2013. 33898

Ben-Ami, Y., Koren, I., Altaratz, O., Kostinski, A., and Lehahn, Y.: Discernible rhythm in the spatio/temporal distributions of transatlantic dust, Atmos. Chem. Phys., 12, 2253–2262, doi:10.5194/acp-12-2253-2012, 2012. 33909, 33910

Boucher, O., Randall, D., Artaxo, P., Bretherton, C., Feingold, G., Forster, P., Kerminen, V.-M., Kondo, Y., Liao, H., Lohmann, U., Rasch, P., Satheesh, S., Sherwood, S., Stevens, B., and

AOD by component from MISR and chemistry models

H. Lee et al.

Title Page

Abstract	Introduction
Conclusions	References
Tables	Figures

◀ ▶|

◀ ▶

Back Close

Full Screen / Esc

Printer-friendly Version

Interactive Discussion

Zhang, X.: Clouds and Aerosols, Book Section 7, Cambridge University Press, Cambridge, UK and New York, NY, USA, doi:10.1017/CBO9781107415324.016, 571–658, 2013. 33899

Braverman, A.: Compressing massive geophysical datasets using vector quantization, J. Comput. Graph. Stat., 11, 44–62, doi:10.1198/106186002317375613, 2002. 33903

Braverman, A. and Di Girolamo, L.: MISR global data products: a new approach, IEEE T. Geosci. Remote, 40, 1626–1636, 2002. 33903

Bristow, C. S., Drake, N., and Armitage, S.: Deflation in the dustiest place on Earth: The Bodélé Depression, Chad, Geomorphology, 105, 50–58, doi:10.1016/j.geomorph.2007.12.014, 2009. 33911

Carboni, E., Thomas, G. E., Sayer, A. M., Siddans, R., Poulsen, C. A., Grainger, R. G., Ahn, C., Antoine, D., Bevan, S., Braak, R., Brindley, H., DeSouza-Machado, S., Deuzé, J. L., Diner, D., Ducos, F., Grey, W., Hsu, C., Kalashnikova, O. V., Kahn, R., North, P. R. J., Salustro, C., Smith, A., Tanré, D., Torres, O., and Veihelmann, B.: Intercomparison of desert dust optical depth from satellite measurements, Atmos. Meas. Tech., 5, 1973–2002, doi:10.5194/amt-5-1973-2012, 2012. 33910

Colarco, P. R., Kahn, R. A., Remer, L. A., and Levy, R. C.: Impact of satellite viewing-swath width on global and regional aerosol optical thickness statistics and trends, Atmos. Meas. Tech., 7, 2313–2335, doi:10.5194/amt-7-2313-2014, 2014. 33908

Diner, D. J., Braswell, B. H., Davies, R., Gobron, N., Hu, J., Jim, Y., Kahn, R. A., Knyazikhin, Y., Loeb, N., Muller, J.-P., Nolin, A. W., Pinty, B., Schaaf, C. B., Seiz, G., and Stroeve, J.: The value of multiangle measurements for retrieving structurally and radiatively consistent properties of clouds, aerosols, and surfaces, Remote Sens. Environ., 97, 495–518, doi:10.1016/j.rse.2005.06.006, 2005a. 33901

Diner, D. J., Martonchik, J. V., Kahn, R. A., Pinty, B., Gobron, N., Nelson, D. L., and Holben, B. N.: Using angular and spectral shape similarity constraints to improve MISR aerosol and surface retrievals over land, Remote Sens. Environ., 94, 155–171, doi:10.1016/j.rse.2004.09.009, 2005b. 33901

Eck, T. F., Holben, B. N., Reid, J. S., Mukelabai, M. M., Piketh, S. J., Torres, O., Jethva, H. T., Hyer, E. J., Ward, D. E., Dubovik, O., Sinyuk, A., Schafer, J. S., Giles, D. M., Sorokin, M., Smirnov, A., and Slutsker, I.: A seasonal trend of single-scattering albedo in southern African biomass-burning particles: Implications for satellite products and estimates of emissions for the world's largest biomass-burning source, J. Geophys. Res., 118, 6414–6432, doi:10.1002/jgrd.50500, 2013. 33908

AOD by component from MISR and chemistry models

H. Lee et al.

Title Page

Abstract | Introduction

Conclusions | References

Tables | Figures

|◄ | ►|

◄ | ►

Back | Close

Full Screen / Esc

Printer-friendly Version

Interactive Discussion

Ganor, E., Osetinsky, I., Stupp, A., and Alpert, P.: Increasing trend of African dust, over 49 years, in the eastern Mediterranean, J. Geophys. Res., 115, D07201, doi:10.1029/2009jd012500, 2010. 33899

Haung, X. H. H., Bian, Q., Ng, W. M., Louie, P. K. K., and Yu, J. Z.: Characterization of $PM_{2.5}$ major components and source investigation in suburban Hong Kong: A one year monitoring study, Aerosol Air Qual. Res., 14, 237–250, doi:10.4209/aaqr.2013.01.0020, 2014. 33909

Higurashi, A. and Nakajima, T.: Detection of aerosol types over the East China Sea near Japan from four-channel satellite data, Geophys. Res. Lett., 29, 1836, doi:10.1029/2002GL015357, 2002. 33900

Holben, B. N., Eck, T. F., Slutsker, I., Tanre, D., Buis, J. P., Setzer, A., Vermote, E., Reagan, J. A., Kaufman, Y. J., Nakajima, T., Lavenu, F., Jankowiak, I., and Smirnov, A.: AERONET – a federated instrument network and data archive for aerosol characterization, Remote Sens. Environ., 66, 1–16, doi:10.1016/S0034-4257(98)00031-5, 1998. 33901

Holzer-Popp, T., Schroedter-Homscheidt, M., Breitkreuz, H., Martynenko, D., and Klüser, L.: Improvements of synergetic aerosol retrieval for ENVISAT, Atmos. Chem. Phys., 8, 7651–7672, doi:10.5194/acp-8-7651-2008, 2008. 33900

Huneeus, N., Schulz, M., Balkanski, Y., Griesfeller, J., Prospero, J., Kinne, S., Bauer, S., Boucher, O., Chin, M., Dentener, F., Diehl, T., Easter, R., Fillmore, D., Ghan, S., Ginoux, P., Grini, A., Horowitz, L., Koch, D., Krol, M. C., Landing, W., Liu, X., Mahowald, N., Miller, R., Morcrette, J.-J., Myhre, G., Penner, J., Perlwitz, J., Stier, P., Takemura, T., and Zender, C. S.: Global dust model intercomparison in AeroCom phase I, Atmos. Chem. Phys., 11, 7781–7816, doi:10.5194/acp-11-7781-2011, 2011. 33905, 33910

Ichoku, C. and Ellison, L.: Global top-down smoke-aerosol emissions estimation using satellite fire radiative power measurements, Atmos. Chem. Phys., 14, 6643–6667, doi:10.5194/acp-14-6643-2014, 2014. 33911, 33912

IPCC: Climate Change 2013: The Physical Science Basis. Contribution of Working Group I to the Fifth Assessment Report of the Intergovernmental Panel on Climate Change, Cambridge University Press, Cambridge, UK and New York, NY, USA, doi:10.1017/CBO9781107415324, 2013. 33899

Kahn, R., Banerjee, P., and McDonald, D.: Sensitivity of multiangle imaging to natural mixtures of aerosols over ocean, J. Geophys. Res., 106, 18219, doi:10.1029/2000jd900497, 2001. 33901

Title Page

Abstract | Introduction

Conclusions | References

Tables | Figures

|◀ | ▶|

◀ | ▶

Back | Close

Full Screen / Esc

Printer-friendly Version

Interactive Discussion

Kahn, R. A. and Gaitley, B. J.: An analysis of global aerosol type as retrieved by MISR, J. Geophys. Res., 120, 4248–4281, doi:10.1002/2015jd023322, 2015. 33901, 33903, 33904

Kahn, R. A., Nelson, D. L., Garay, M. J., Levy, R. C., Bull, M. A., Diner, D. J., Martonchik, J. V., Paradise, S. R., Hansen, E. G., and Remer, L. A.: MISR aerosol product attributes and statistical comparisons with MODIS, IEEE T. Geosci. Remote, 47, 4095–4114, doi:10.1109/TGRS.2009.2023115, 2009. 33905

Kahn, R. A., Gaitley, B. J., Garay, M. J., Diner, D. J., Eck, T. F., Smirnov, A., and Holben, B. N.: Multiangle Imaging SpectroRadiometer global aerosol product assessment by comparison with the Aerosol Robotic Network, J. Geophys. Res., 115, D23209, doi:10.1029/2010jd014601, 2010. 33901, 33903, 33904, 33906, 33910

Kalashnikova, O. V., Kahn, R., Sokolik, I. N., and Li, W. H.: Ability of multiangle remote sensing observations to identify and distinguish mineral dust types: Optical models and retrievals of optically thick plumes, J. Geophys. Res., 110, D18S14, doi:10.1029/2004jd004550, 2005. 33906

Kim, J., Lee, J., Lee, H. C., Higurashi, A., Takemura, T., and Song, C. H.: Consistency of the aerosol type classification from satellite remote sensing during the Atmospheric Brown Cloud-East Asia Regional Experiment campaign, J. Geophys. Res., 112, D22S33, doi:10.1029/2006jd008201, 2007. 33900, 33908

Koven, C. D. and Fung, I.: Identifying global dust source areas using high-resolution land surface form, J. Geophys. Res., 113, D22204, doi:10.1029/2008JD010195, 2008. 33909

Lamarque, J.-F., Shindell, D. T., Josse, B., Young, P. J., Cionni, I., Eyring, V., Bergmann, D., Cameron-Smith, P., Collins, W. J., Doherty, R., Dalsoren, S., Faluvegi, G., Folberth, G., Ghan, S. J., Horowitz, L. W., Lee, Y. H., MacKenzie, I. A., Nagashima, T., Naik, V., Plummer, D., Righi, M., Rumbold, S. T., Schulz, M., Skeie, R. B., Stevenson, D. S., Strode, S., Sudo, K., Szopa, S., Voulgarakis, A., and Zeng, G.: The Atmospheric Chemistry and Climate Model Intercomparison Project (ACCMIP): overview and description of models, simulations and climate diagnostics, Geosci. Model Dev., 6, 179–206, doi:10.5194/gmd-6-179-2013, 2013. 33902

Lee, H., Kim, H., Honda, Y., Lim, Y. H., and Yi, S.: Effect of Asian dust storms on daily mortality in seven metropolitan cities of Korea, Atmos. Environ., 79, 510–517, doi:10.1016/j.atmosenv.2013.06.046, 2013. 33899, 33909

Title Page

Abstract | Introduction

Conclusions | References

Tables | Figures

|◀ | ▶|

◀ | ▶

Back | Close

Full Screen / Esc

Printer-friendly Version

Interactive Discussion

Levy, R. C., Leptoukh, G. G., Kahn, R., Zubko, V., Gopalan, A., and Remer, L. A.: A critical look at deriving monthly Aerosol Optical depth from satellite data, IEEE T. Geosci. Remote, 47, 2942–2956, doi:10.1109/Tgrs.2009.2013842, 2009. 33908

Levy, R. C., Mattoo, S., Munchak, L. A., Remer, L. A., Sayer, A. M., Patadia, F., and Hsu, N. C.: The Collection 6 MODIS aerosol products over land and ocean, Atmos. Meas. Tech., 6, 2989–3034, doi:10.5194/amt-6-2989-2013, 2013. 33908

Li, G. H., Wang, Y., Lee, K. H., Diao, Y. W., and Zhang, R. Y.: Increased winter precipitation over the North Pacific from 1984–1994 to 1995–2005 inferred from the Global Precipitation Climatology Project, Geophys. Res. Lett., 35, L13821, doi:10.1029/2008gl034668, 2008. 33899

Li, S., Garay, M. J., Chen, L., Rees, E., and Liu, Y.: Comparison of GEOS-Chem aerosol optical depth with AERONET and MISR data over the contiguous United States, J. Geophys. Res., 118, 11228–11241, doi:10.1002/jgrd.50867, 2013. 33901

Li, S., Kahn, R., Chin, M., Garay, M. J., and Liu, Y.: Improving satellite-retrieved aerosol microphysical properties using GOCART data, Atmos. Meas. Tech., 8, 1157–1171, doi:10.5194/amt-8-1157-2015, 2015. 33901

Liousse, C., Guillaume, B., Grégoire, J. M., Mallet, M., Galy, C., Pont, V., Akpo, A., Bedou, M., Castéra, P., Dungall, L., Gardrat, E., Granier, C., Konaré, A., Malavelle, F., Mariscal, A., Mieville, A., Rosset, R., Serça, D., Solmon, F., Tummon, F., Assamoi, E., Yoboué, V., and Van Velthoven, P.: Updated African biomass burning emission inventories in the framework of the AMMA-IDAF program, with an evaluation of combustion aerosols, Atmos. Chem. Phys., 10, 9631–9646, doi:10.5194/acp-10-9631-2010, 2010. 33912

Liu, S., Aiken, A. C., Arata, C., Dubey, M. K., Stockwell, C. E., Yokelson, R. J., Stone, E. A., Jayarathne, T., Robinson, A. L., DeMott, P. J., and Kreidenweis, S. M.: Aerosol single scattering albedo dependence on biomass combustion efficiency: laboratory and field studies, Geophys. Res. Lett., 41, 742–748, doi:10.1002/2013gl058392, 2014. 33906

Lu, Z., Streets, D. G., Zhang, Q., Wang, S., Carmichael, G. R., Cheng, Y. F., Wei, C., Chin, M., Diehl, T., and Tan, Q.: Sulfur dioxide emissions in China and sulfur trends in East Asia since 2000, Atmos. Chem. Phys., 10, 6311–6331, doi:10.5194/acp-10-6311-2010, 2010. 33899

Marlier, M. E., Voulgarakis, A., Shindell, D. T., Faluvegi, G., Henry, C. L., and Randerson, J. T.: The role of temporal evolution in modeling atmospheric emissions from tropical fires, Atmos. Environ., 89, 158–168, doi:10.1016/j.atmosenv.2014.02.039, 2014. 33912

Matichuk, R. I., Colarco, P. R., Smith, J. A., and Toon, O. B.: Modeling the transport and optical properties of smoke aerosols from African savanna fires during the Southern African

Title Page

Abstract | Introduction

Conclusions | References

Tables | Figures

|◄ | ►|

◄ | ►

Back | Close

Full Screen / Esc

Printer-friendly Version

Interactive Discussion

Regional Science Initiative campaign (SAFARI 2000), J. Geophys. Res., 112, D08203, doi:10.1029/2006JD007528, 2007. 33912

Myhre, G., Samset, B. H., Schulz, M., Balkanski, Y., Bauer, S., Berntsen, T. K., Bian, H., Bellouin, N., Chin, M., Diehl, T., Easter, R. C., Feichter, J., Ghan, S. J., Hauglustaine, D., Iversen, T., Kinne, S., Kirkevåg, A., Lamarque, J.-F., Lin, G., Liu, X., Lund, M. T., Luo, G., Ma, X., van Noije, T., Penner, J. E., Rasch, P. J., Ruiz, A., Seland, Ø., Skeie, R. B., Stier, P., Takemura, T., Tsigaridis, K., Wang, P., Wang, Z., Xu, L., Yu, H., Yu, F., Yoon, J.-H., Zhang, K., Zhang, H., and Zhou, C.: Radiative forcing of the direct aerosol effect from AeroCom Phase II simulations, Atmos. Chem. Phys., 13, 1853–1877, doi:10.5194/acp-13-1853-2013, 2013. 33902

Nabat, P., Somot, S., Mallet, M., Chiapello, I., Morcrette, J. J., Solmon, F., Szopa, S., Dulac, F., Collins, W., Ghan, S., Horowitz, L. W., Lamarque, J. F., Lee, Y. H., Naik, V., Nagashima, T., Shindell, D., and Skeie, R.: A 4-D climatology (1979–2009) of the monthly tropospheric aerosol optical depth distribution over the Mediterranean region from a comparative evaluation and blending of remote sensing and model products, Atmos. Meas. Tech., 6, 1287–1314, doi:10.5194/amt-6-1287-2013, 2013. 33900

Omar, A. H., Winker, D. M., Vaughan, M. A., Hu, Y., Trepte, C. R., Ferrare, R. A., Lee, K.-P., Hostetler, C. A., Kittaka, C., Rogers, R. R., Kuehn, R. E., and Liu, Z.: The CALIPSO automated aerosol classification and lidar ratio selection algorithm, J. Atmos. Ocean. Tech., 26, 1994–2014, doi:10.1175/2009jtecha1231.1, 2009. 33900

Ott, W. R.: A physical explanation of the lognormality of pollutant concentrations, JAPCA J. Air Waste Ma., 40, 1378–1383, doi:10.1080/10473289.1990.10466789, 1990. 33908

Prospero, J. M., Ginoux, P., Torres, O., Nicholson, S. E., and Gill, T. E.: Environmental characterization of global sources of atmospheric soil dust identified with the Nimbus 7 Total Ozone Mapping Spectrometer (TOMS) absorbing aerosol product, Rev. Geophys., 40, 1002, doi:10.1029/2000rg000095, 2002. 33910

Regayre, L. A., Pringle, K. J., Booth, B. B. B., Lee, L. A., Mann, G. W., Browse, J., Woodhouse, M. T., Rap, A., Reddington, C. L., and Carslaw, K. S.: Uncertainty in the magnitude of aerosol-cloud radiative forcing over recent decades, Geophys. Res. Lett., 41, 9040–9049, doi:10.1002/2014gl062029, 2014. 33899

Ridley, D. A., Heald, C. L., and Ford, B.: North African dust export and deposition: A satellite and model perspective, J. Geophys. Res., 117, D02202, doi:10.1029/2011JD016794, 2012. 33909

Russell, P. B., Kacenelenbogen, M., Livingston, J. M., Hasekamp, O. P., Burton, S. P., Schuster, G. L., Johnson, M. S., Knobelspiesse, K. D., Redemann, J., Ramachandran, S., and Holben, B.: A multiparameter aerosol classification method and its application to retrievals from spaceborne polarimetry, J. Geophys. Res., 119, 9838–9863, doi:10.1002/2013jd021411, 2014. 33900

Satoh, M., Matsuno, T., Tomita, H., Miura, H., Nasuno, T., and Iga, S.: Nonhydrostatic icosahedral atmospheric model (NICAM) for global cloud resolving simulations, J. Comput. Phys., 227, 3486–3514, doi:10.1016/j.jcp.2007.02.006, 2008. 33902

Satoh, M., Tomita, H., Yashiro, H., Miura, H., Kodama, C., Seiki, T., Noda, A., Yamada, Y., Goto, D., Sawada, M., Miyoshi, T., Niwa, Y., Hara, M., Ohno, T., Iga, S.-i., Arakawa, T., Inoue, T., and Kubokawa, H.: The Non-hydrostatic Icosahedral Atmospheric Model: description and development, Prog. Earth Planet. Sci., 1, 18, doi:10.1186/s40645-014-0018-1, 2014. 33902

Schulz, M., Textor, C., Kinne, S., Balkanski, Y., Bauer, S., Berntsen, T., Berglen, T., Boucher, O., Dentener, F., Guibert, S., Isaksen, I. S. A., Iversen, T., Koch, D., Kirkevåg, A., Liu, X., Montanaro, V., Myhre, G., Penner, J. E., Pitari, G., Reddy, S., Seland, Ø., Stier, P., and Takemura, T.: Radiative forcing by aerosols as derived from the AeroCom present-day and pre-industrial simulations, Atmos. Chem. Phys., 6, 5225–5246, doi:10.5194/acp-6-5225-2006, 2006. 33902

Shindell, D. T., Lamarque, J.-F., Schulz, M., Flanner, M., Jiao, C., Chin, M., Young, P. J., Lee, Y. H., Rotstayn, L., Mahowald, N., Milly, G., Faluvegi, G., Balkanski, Y., Collins, W. J., Conley, A. J., Dalsoren, S., Easter, R., Ghan, S., Horowitz, L., Liu, X., Myhre, G., Nagashima, T., Naik, V., Rumbold, S. T., Skeie, R., Sudo, K., Szopa, S., Takemura, T., Voulgarakis, A., Yoon, J.-H., and Lo, F.: Radiative forcing in the ACCMIP historical and future climate simulations, Atmos. Chem. Phys., 13, 2939–2974, doi:10.5194/acp-13-2939-2013, 2013. 33899

Streets, D. G. and Waldhoff, S. T.: Present and future emissions of air pollutants in China: SO_2, NO_x, and CO, Atmos. Environ., 34, 363–374, 2000. 33907

Streets, D. G., Fu, J. S., Jang, C. J., Hao, J., He, K., Tang, X., Zhang, Y., Wang, Z., Li, Z., Zhang, Q., Wang, L., Wang, B., and Yu, C.: Air quality during the 2008 Beijing Olympic Games, Atmos. Environ., 41, 480–492, 2007. 33907

Suzuki, K., Nakajima, T., Satoh, M., Tomita, H., Takemura, T., Nakajima, T. Y., and Stephens, G. L.: Global cloud-system-resolving simulation of aerosol effect on warm clouds, Geophys. Res. Lett., 35, L19817, doi:10.1029/2008gl035449, 2008. 33902, 33905

Takemura, T., Nakajima, T., Dubovik, O., Holben, B. N., and Kinne, S.: Single-scattering albedo and radiative forcing of various aerosol species with a global three-dimensional model, J. Climate, 15, 333–352, doi:10.1175/1520-0442(2002)015<0333:SSAARF>2.0.CO;2, 2002. 33902

Takemura, T., Nozawa, T., Emori, S., Nakajima, T. Y., and Nakajima, T.: Simulation of climate response to aerosol direct and indirect effects with aerosol transport-radiation model, J. Geophys. Res., 110, D02202, doi:10.1029/2004jd005029, 2005. 33902, 33912

Taylor, K. E., Stouffer, R. J., and Meehl, G. A.: An overview of CMIP5 and the experiment design, B. Am. Meteorol. Soc., 93, 485–498, doi:10.1175/BAMS-D-11-00094.1, 2012. 33902

Teixeira, J., Waliser, D., Ferraro, R., Gleckler, P., Lee, T., and Potter, G.: Satellite observations for CMIP5: The genesis of Obs4MIPs, B. Am. Meteorol. Soc., 95, 1329–1334, doi:10.1175/Bams-D-12-00204.1, 2014. 33902

Tilmes, S., Lamarque, J.-F., Emmons, L. K., Kinnison, D. E., Ma, P.-L., Liu, X., Ghan, S., Bardeen, C., Arnold, S., Deeter, M., Vitt, F., Ryerson, T., Elkins, J. W., Moore, F., Spackman, J. R., and Val Martin, M.: Description and evaluation of tropospheric chemistry and aerosols in the Community Earth System Model (CESM1.2), Geosci. Model Dev., 8, 1395–1426, doi:10.5194/gmd-8-1395-2015, 2015. 33899

van der Werf, G. R., Randerson, J. T., Giglio, L., Collatz, G. J., Mu, M., Kasibhatla, P. S., Morton, D. C., DeFries, R. S., Jin, Y., and van Leeuwen, T. T.: Global fire emissions and the contribution of deforestation, savanna, forest, agricultural, and peat fires (1997–2009), Atmos. Chem. Phys., 10, 11707–11735, doi:10.5194/acp-10-11707-2010, 2010. 33911, 33912

Veira, A., Kloster, S., Schutgens, N. A. J., and Kaiser, J. W.: Fire emission heights in the climate system – Part 2: Impact on transport, black carbon concentrations and radiation, Atmos. Chem. Phys., 15, 7173–7193, doi:10.5194/acp-15-7173-2015, 2015. 33912

Wang, L., Jang, C., Zhang, Y., Wang, K., Zhang, Q., Streets, D., Fu, J., Lei, Y., Schreifels, J., He, K., Hao, J., Lam, Y.-F., Lin, J., Meskhidze, N., Voorhees, S., Evarts, D., and Phillips, S.: Assessment of air quality benefits from national air pollution control policies in China. Part II: Evaluation of air quality predictions and air quality benefits assessment, Atmos. Environ., 44, 3449–3457, doi:10.1016/j.atmosenv.2010.05.058, 2010. 33907, 33908, 33909

Title Page

Abstract | Introduction

Conclusions | References

Tables | Figures

|◀ | ▶|

◀ | ▶

Back | Close

Full Screen / Esc

Printer-friendly Version

Interactive Discussion

Wang, Y., Wang, M. H., Zhang, R. Y., Ghan, S. J., Lin, Y., Hu, J. X., Pan, B. W., Levy, M.,
Jiang, J. H., and Molina, M. J.: Assessing the effects of anthropogenic aerosols on Pacific
storm track using a multiscale global climate model, P. Natl. Acad. Sci. USA, 111, 6894–
6899, doi:10.1073/pnas.1403364111, 2014. 33899

5   Yu, H. B., Remer, L. A., Chin, M., Bian, H. S., Kleidman, R. G., and Diehl, T.: A satellite-based
assessment of transpacific transport of pollution aerosol, J. Geophys. Res., 113, D14S12,
doi:10.1029/2007jd009349, 2008. 33906

Zhang, R. Y., Li, G. H., Fan, J. W., Wu, D. L., and Molina, M. J.: Intensification of Pa-
cific storm track linked to Asian pollution, P. Natl. Acad. Sci. USA, 104, 5295–5299,
10   doi:10.1073/pnas.0700618104, 2007. 33899

Table 1. Combination of AOD by component for comparison between MISR and SPRINTARS. The names of aerosol components in MISR are from Table 1 in Kahn et al. (2015).

MISR	SPRINTARS
weakly+strongly absorbing aerosols : sph_absorb_0.12_ssa_green_09 + sph_absorb_0.12_ssa_green_08	carbonaceous aerosols
medium + coarse non-spherical aerosols : medium_grains + coarse_spheroids	dust
very small + small + medium non-absorbing aerosols : sph_nonabsorb_0.06 + sph_nonabsorb_0.12 + sph_nonabsorb_0.26	sulfate

Figure 1. A scatter plot of absorbing AOD and non-absorbing AOD and their histograms over East Asia (117.5–127.5° E, 32.5–42.5° N) in April between 2000 and 2014. The AOD data are from MISR Version 1 Level 3 Joint Aerosol product (JOINT_AS) based on the Version 22 operational Level 2 aerosol retrievals. The two histograms for non-absorbing AOD and absorbing AOD are scaled to show a probability mass function (PMF) so that the total area of the bars in each histogram becomes one.
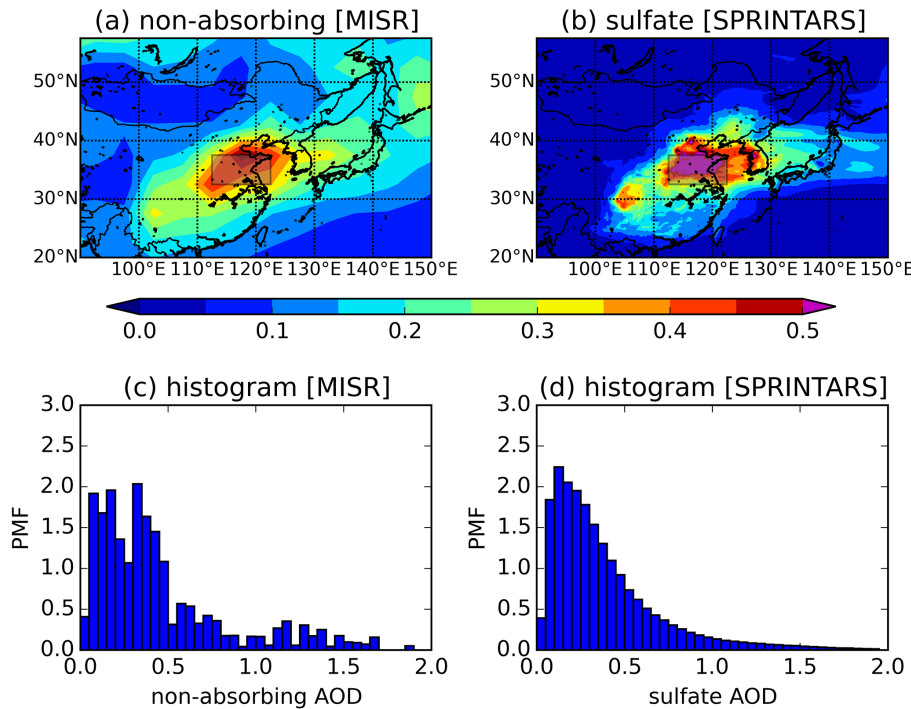
Figure 2. (a) Climatological mean optical depth of the non-absorbing aerosols in MISR and **(b)** sulfate aerosol optical depth in SPRINTAS over East Asia (112.5–122.5° E, 32.5–37.5° N). Spatio-temporal distributions of **(c)** the non-absorbing AOD in MISR for 15 Julys between 2000 and 2014 and **(d)** sulfate AOD in SPRINTARS for July 2006, covering the boxed emission source region are displayed.
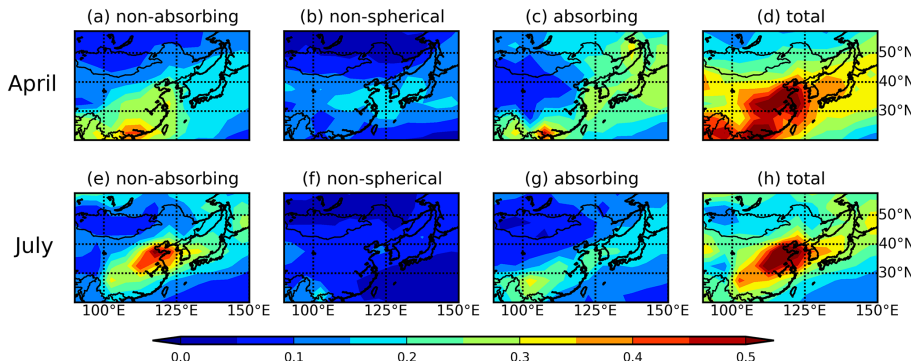
Figure 3. Map of average MISR optical depth of absorbing aerosols, non-spherical, non-absorbing aerosols and total aerosols in April **(a–d)** and July **(e–h)**.
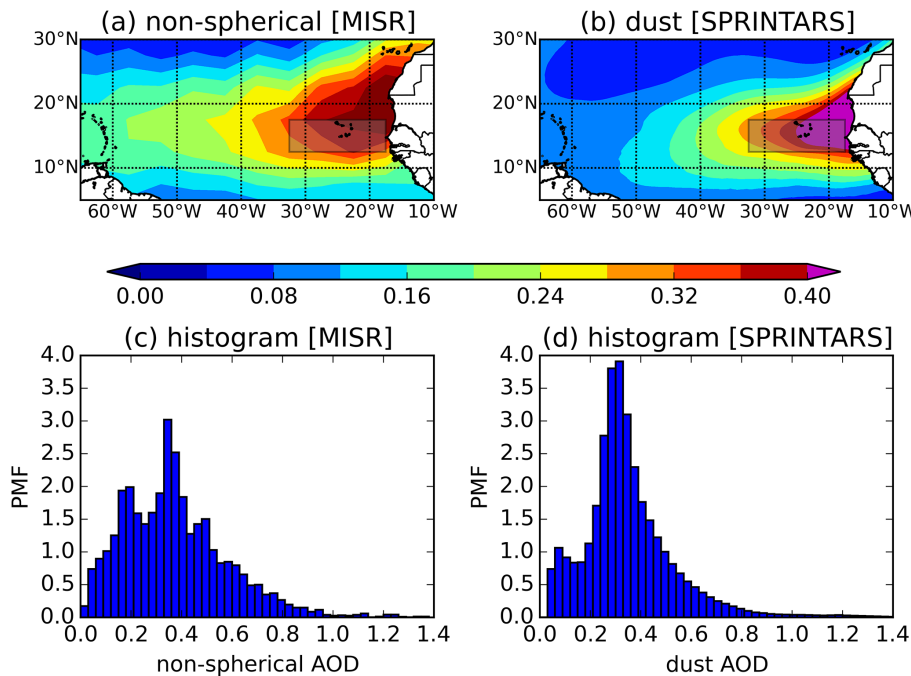
Figure 4. (a) Climatological mean optical depth of the non-spherical aerosols in MISR and **(b)** SPRINTARS over Sahara Desert (32.5° E–17.5° W, 12.5–17.5° N). Spatio-temporal distributions of **(c)** the non-spherical AOD in MISR for 15 Julys between 2000 and 2014 and **(d)** dust AOD in SPRINTARS for July 2006, covering the boxed region off the coast are displayed.
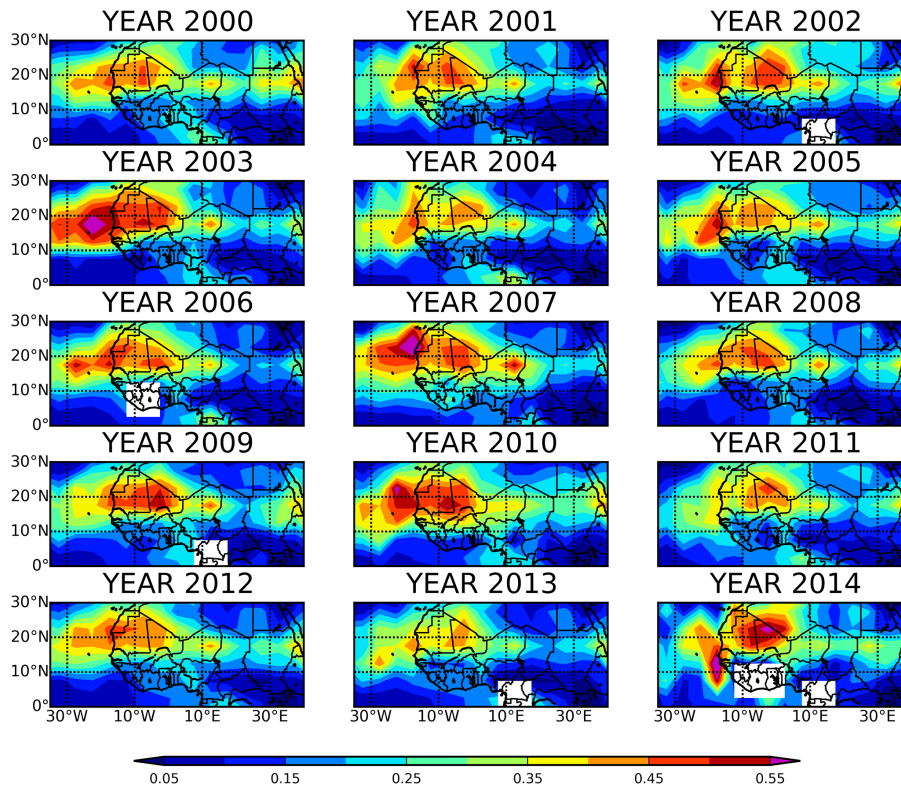
Figure 5. Monthly mean optical depth of the dust aerosols from MISR in July for 15 years between 2000 and 2014.

Title Page

Abstract | Introduction

Conclusions | References

Tables | Figures

|◀ | ▶|

◀ | ▶

Back | Close

Full Screen / Esc

Printer-friendly Version

Interactive Discussion
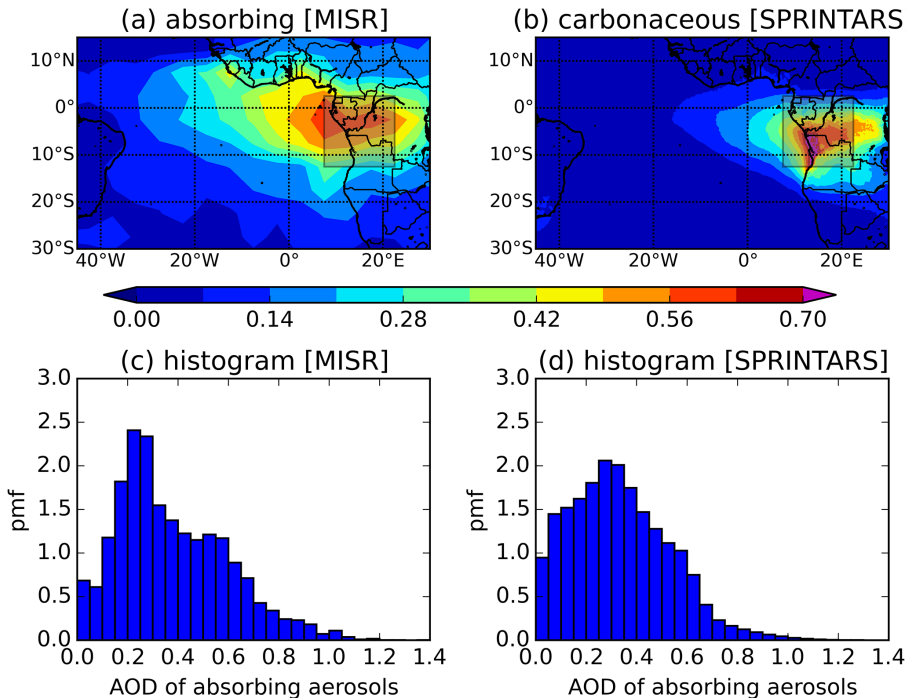
Figure 6. (a) Climatological mean optical depth of the absorbing aerosols in MISR and **(b)** carbonaceous aerosols optical depth in SPRINTAS over West Africa (7.5–22.5° E, 12.5° S–2.5° N). Spatio-temporal distributions of **(c)** the absorbing AOD in MISR for 15 Julys between 2000 and 2014 and **(d)** carbonaceous AOD in SPRINTARS for July 2006, covering the boxed emission source region are displayed.